RSC Advances

ROYAL SOCIETY OF CHEMISTRY

www.rsc.org/advances

Nanosheet-based 3D hierarchical ZnO structure decorated with Au nanoparticle for enhanced electrochemical detection of dopamine

Linxia Fang[a,b], Kejing Huang[b], Baoling Zhang[a], Bing Liu[b], Yujie Liu[b], Qiuyu Zhang[a,*]

[a]*Department of Applied Chemistry, School of Science, Northwestern Polytechnical University, 710072 Xi'an, China*

[b]*College of Chemistry and Chemical Engineering, Xinyang Normal University, 464000 Xinyang ,China*

* Corresponding author. Tel: +86 13152160629
E-mail address: qyzhang@nwpu.edu.cn

Abstract: The biocompatible Au-ZnO nanocomposite was used to fabricate a sensitive sensor for the detection of dopamine (DA). High-density Au nanoparticles (AuNPs) were homogeneously loaded onto nanosheet-based three-dimensionally (3D) hierarchical ZnO matrix. High special surface area of nanosheet-based three-dimensionally (3D) hierarchical ZnO favored the high density load of AuNPs, which helped efficiently catalyze the oxidation of DA. The Au-ZnO nanocomposite was characterized by scanning electron microscopy (SEM), energy dispersive spectrometer (EDS), transmission electron microscopy (TEM), X-ray powder diffraction (XRD) and electrochemical impedance spectroscopy (EIS). The electrocatalytic activity toward the oxidation of dopamine was investigated by cyclic voltammetry (CV) and differential pulse voltammetry (DPV). The sensors exhibited sensitive responses to DA with a linear range of 0.1-300 μM and a detection limit of 0.02 μM based on S/N = 3. The good analytical performance and long-term stability of the proposed sensor can be attributed to the synergistic effect of the nanosheet-based ZnO structure and gold nanoparticles on the electrochemical oxidation of dopamine.

Keywords: nanosheet-based; 3D hierarchical ZnO; sensor; dopamine

1. Introduction

Dopamine (DA) is an important neurotransmitter that belongs to the catecholamines group and has a great influence on the central nervous, renal, hormonal and cardiovascular systems [1, 2]. Abnormal levels of dopamine may result in a variety of diseases, such as Schizophrenia, Huntington's disease, Parkinson's disease, and dementia among many others [3]. As a result, detecting and monitoring

the concentration of DA play an important role in disease diagnosis. Many analytical methods based on different principles, including gas chromatography coupled to mass spectrometry (GC–MS)[4], ultra-high performance liquid chromatography coupled to mass spectrometry (UHPLC–MS/MS)[5] and spectrophotometry[6] have been developed for detection of DA and showed a low detection limit, high sensitivity and selectivity. However, they are probably unsuitable for routine analysis because of large-scale expensive instrument, troublesome and time-consuming pretreatment, the use of large quantity of solvent.

The fact that DA is electrochemically active (oxidizable) allows electrochemical techniques to be employed for the detection of DA levels. Electrochemical analytical technique for DA determination is a good alternative due to low cost, easy operation, fast response, high sensitivity and environmental friendliness [7-10]. However, uric acid (UA) and ascorbic acid (AA) are coexisted with dopamine in the extracellular fluids of the central nervous system in mammals. These electroactive biomolecules will interfere with normal signals of DA unavoidably because they can be oxidized at potentials close to that of dopamine at the most commonly used solid electrodes [11]. Obviously, it is necessary to develop selective and sensitive techniques to resolve these problems. Although, various modified electrodes have been employed to enhance the voltammetric selectivity and sensitivity towards dopamine determination [12-16], it is still attractive to develop novel materials for sensitive determination of DA in the electrochemical field.

ZnO is a versatile n-type metal oxide semiconductor material with a direct wide

band gap (3.37 eV) and large exciton binding energy (60 meV) at room temperature. It has been extensively used in the fabrication of electrical, optical and photovoltaic devices, heterogeneous catalysis, storage media, gas sensing and field-emission (FE) emitters [17-22]. Furthermore, due to its good biocompatibility, notoxity and inexpensiveness, ZnO has been widely used in the fabrication of electrochemical biosensors [23-28]. In these biosensors, ZnO was employed as support matrix on the modified electrodes for electrocatalysis of various bimolecular, which can facilitate the direct electron transfer and enhance the catalytic activity.

Considering its wide applications, various ZnO nanostructures including wires, rods, tubes, hollow nanospheres, etc. have been prepared during the past few years [29]. Among various shapes of nanomaterials, nanosheet has attracted intensive interests as sheet-like materials with predominantly exposed crystal facets may exhibit improved catalytic performance over their wire-like or spherical structures due to their high surface-to-volume ratio [30, 31]. 3D hierarchical ZnO structure is a very promising sensing material because of its advantageous features including low density, high surface area, nanosheet structure and good permeability.

Moreover, in order to increase the current response of the modified sensor, composite metallic nanoparticles with substrates have attracted much interest in the construction of electrochemical sensors. Among the metallic nanoparticles, gold nanoparticles are widely used in electrochemistry because of their biocompatibility, large specific surface area, high surface free energy and suitability for constructing electrochemical biosensors [32, 33]. Biosensors constructed with AuNPs have been

applied to determine various electroactive molecules, such as dopamine (DA) [34, 35], uric acid (2, 6, 8-trihydroxypurine, UA) [36], ascorbic acid (AA) [37, 38], guanine (G) and adenine (A) [39]. Unfortunately, most of the AuNPs immobilization matrices obtained thus far showed limited responses to the target molecules [40, 41]. Furthermore, AuNPs are fixed on the matrix surface or deposited into it in a 2D distribution, which produce poor responses to target molecules due to lower AuNPs surface areas.

In this work, 3D hierarchical ZnO crystals were prepared by a simple hydrolysis method, and then Au-ZnO nanocomposite was synthesized by employing ZnO as a matrix upon which AuNPs were formed via in situ reduction of $HAuCl_4$. A novel electrochemical sensing platform for sensitive detection of DA was constructed by casting Au-ZnO composites on glassy carbon electrode (GCE). Taking advantages of high surface area of nanosheet-based hierarchical ZnO crystals and the high-density conducting AuNPs, this electrochemical sensor showed a low detection limit and wide linear range, and it had been applied for assay of DA in human urine samples with satisfactory results.

2. Experimental

2.1. Reagents and materials

Chloroauric acid tetrahydrate ($HAuCl_4 \cdot 4H_2O$), trisodium citrate, ascorbic acid (AA) and uric acid (UA) were purchased from Shanghai Chemical Reagent Co., Ltd. (Shanghai, China). Dopamine (DA) was purchased from Sigma-Aldrich (USA). Human urine sample was provided by volunteer. Other chemicals used were of

analytical grade and purchased from China National Pharmaceutical Industry Corporation Ltd. Phosphate buffer solution (PBS, 0.1 M, pH 7.0) was prepared from NaH_2PO_4 and Na_2HPO_4. All aqueous solutions were prepared with pure water obtained from a Milli-Q Plus system (Millipore).

2.2. Preparation of nanosheet-based ZnO porous microspheres

The preparation and the growth mechanism of nanosheet-based three-dimensionally (3D) hierarchical ZnO have been demonstrated in our previous work [42]. In a typical synthesis, an equimolar ratio of zinc acetate dihydrate (25 mM） and hexamine (HMTA) (25 mM) was dissolved into 50 mL of deionized water with subsequent addition of trisodium citrate (5 mM), followed by stirring at room temperature for 20 min. The final mixture was transferred to a 100 mL Teflon-stainless beaker for hydrolysis reaction at 90 ℃ in an oven for 6 h. After completion of the reaction, cooling to room temperature naturally, the resulting white precipitate was collected by centrifugation and purified by washing with deionized water and absolute ethanol several times and dried at 60 ℃ for 24 h.

2.3. Preparation of Au-ZnO nanocomposite

The prepared three-dimensionally (3D) hierarchical ZnO was dispersed into 10 mL water by ultrasonication. Then, 140 μL freshly prepared $HAuCl_4 \cdot 4H_2O$ aqueous solution (30 mM) was added into the dispersion by stirring. Subsequently, 0.25 mL of sodium borohydride ($NaBH_4$) aqueous solution (0.2 M) was added drop by drop into the mixture solution with vigorous stirring at room temperature for 30 min. Finally, the products were collected by centrifugation and were washed with water and

absolute ethanol several times to produce Au dotted nanosheet-based hierarchical ZnO (Au-ZnO nanocomposite). The precipitate was redispersed by 1 mL water and stored at 4 ℃in a refrigerator when not in use.

2.4. Preparation of modified electrode

Prior to electrode modification the GCE was polished with 0.05 μm alumina slurry and Buehler polishing cloth. It was then washed with water and ultrasonicated for 3 min each in water and ethanol to remove any adsorbed alumina particles or dirt from the electrode surface and finally dried in nitrogen airflow. 5 μL of Au-ZnO water dispersion was drop casted onto the pre-cleaned GCE and dried at room temperature. For comparison, ZnO/GCE was prepared by adopting the similar procedures and used for further investigation.

2.5. Instruments and measurements

High-resolution transmission electron microscopy (HRTEM) and scanning electron microscopy (SEM) images were obtained by employing a JEOL 2100F microscope, and a Hitachi S4800 scanning electron microscope (SEM). X-ray powder diffraction (XRD) pattern was operated on a Japan RigakuD/Maxr-A X-ray diffractometer equipped with graphite monochromatized high-intensity Cu Kα radiation (λ= 1.54178Å). The pH measurements were made with a pH meter Leici Devices Factory of Shanghai, China. All electrochemical experiments were carried out on a CHI 660D Electrochemical Workstation (Shanghai, CH Instruments, China) with a conventional three-electrode system composed of a platinum wire electrode as the auxiliary electrode, a saturated calomel electrode (SCE) as the reference electrode

and a modified GCE (3.0 mm in diameter) as the working electrode. All of the potentials in this article were with respect to SCE. Cyclic voltammetry (CV) method was performed in the potential range from -0.2 to +0.8 V at a scan rate of 100 mV s^{-1}. Differential pulse voltammetry (DPV) measurement was performed in the scan range from -0.2 to +0.6 V, with the pulse amplitude of 50 mV, pulse width of 50 ms and pulse period of 0.2 s. Electrochemical impedance spectroscopy (EIS) experiment was carried out in a 10.0 mL aqueous solution containing 5 mM of $[Fe(CN)_6]^{3-/4-}$ and 0.1 M of KCl at a potential of 0.2 V over the frequency range from 0.1 Hz to 100 kHz, using an amplitude of 5 mV. Every experiment was parallel performed three times (n=3).

3. Results and discussions

3.1. Characterization of Au-ZnO nanocomposite

The surface morphologies of the ZnO and Au-ZnO nanocomposite were examined by SEM, as shown in Fig. 1. The low magnification SEM image of the prepared ZnO, as shown in Fig. 1a, featured nanosheet-based microsphere structure and a good dispersion with an average diameter of about 2-3 μm. From the high magnification

Fig. 1

SEM image, the microsphere is built up of nanosheet with the thickness of several nanometers as depicted in Fig. 1b. Fig. 1c shows a typical SEM image of Au-ZnO nanocomposite. It is can be seen that a high coverage of AuNPs deposited on the surface of ZnO nanosheet which leaded to the porosity degrade and the surface illegible. The Energy Dispersive Spectrometer (EDS) of the Au-ZnO nanohybride is

shown in Fig. 1 d. The data supports the in situ formation of AuNPs on the surfaces of ZnO nanosheet.

TEM and HRTEM were performed to further reveal the morphology of Au-ZnO nanocomposite. Fig.1e shows HRTEM image of Au-ZnO nanocomposite, revealing the distinct crystal lattic of AuNPs. It could also be seen from TEM image of Au-ZnO nanocomposite shown in the inset of Fig.1e that the individual torispherical AuNPs with diameters of 5-10 nm are dispersed on the surface of ZnO nanosheet. Large specific surface areas of the 3D nanosheet-based porous ZnO hierarchical structure, combining with specific electronic and catalytic properties of AuNPs, could be a good candidate for electrochemical sensor construction.

Fig. 1f shows the XRD patterns of ZnO (curve a) and Au-ZnO nanocomposite (curve b). The major diffraction peaks shown in curve a can be indexed to a phase from crystalline ZnO based on the data from the JCPDS file (21-1486). The three additional peaks locating at 38.16°, 44.51° and 64.54° in curve b are assigned to (111), (200) and (220) planes reflection of AuNPs (JCPDS Card No. 65-2870), which proves the formation of crystalline AuNPs on the ZnO microspheres. These results are in good agreement with the data from the EDS.

EIS was employed to study the interfacial electron-transfer resistance (R*ct*) at the modified electrodes. The Nyquist plots of the bare GCE, ZnO/GCE and Au-ZnO/GCE in the presence of redox probe $[Fe(CN)_6]^{4-/3-}$ are shown in Fig. 2. The Nyquist plot of EIS includes a semicircle portion at high frequencies corresponding to the electron-transfer-limited process and a linear part at low frequency range

198 **Fig. 2**

199 representing the diffusion-limited process. The diameter of semicircle portion is equal
200 to the electron transfer resistance (R*ct*). The impedance of the sensing system can be
201 roughly modeld by the Randles equivalent circuit, as shown in Fig. 2 (inset A). As
202 shown, there is a very small semicircle domain in the Nyquist plot of EIS on the bare
203 GCE (curve a), implying a very low electron transfer resistance to the redox-probe
204 dissolved in the electrolyte solution. EIS of ZnO (curve c) exhibits an enlarged
205 semicircle representing a bigger R*ct*. This result suggests that a layer of ZnO film has
206 formed on the surface of GCE, and hinder the charge transfer from the redox probe of
207 $[Fe(CN)_6]^{3-/4-}$ to the GCE surface due to the poor conductivity of ZnO. However, in
208 the case of Au-ZnO/GCE (curve b), the diameter of the semicircle was observed to
209 decrease obviously in comparison with ZnO/GCE. This phenomenon implies that
210 AuNPs were successfully introduced onto the surface of ZnO, and the existence of
211 AuNPs could improve electrical conductivity and accelerate the electron transfer rate.

212 **3.2. Electrochemical behavior of DA at the modified electrodes**

213 In order to verify the electrocatalytic activity of the Au-ZnO/GCE toward the
214 oxidation of DA, CV scan was carried in the absence or presence of DA. Fig. 3
215 shows CVs of Au-ZnO/GCE whiout DA (a) and ZnO/GCE (b), GCE (c),
216 Au-ZnO/GCE (d) for 50 μM DA in 0.1 M phosphate buffer solution (PBS, pH 7.0). It
217 is clear that in the absence of DA, no oxidation response can be seen on the
218 Au-ZnO/GCE. Upon adding 50 μM DA, the bare GCE shows a couple of redox peak
219 with a peak-to-peak (△Ep) of 205 mV. By comparison, the ZnO/GCE gave a

relatively small redox current and a big peak potentials separation (△Ep=302mV)

Fig. 3

than those recorded at the bare GCE. However, at the Au-ZnO/GCE, the redox currents was greatly enhanced and peak potentials separation (∆Ep=152 mV) was greatly reduced with a well-defined and stable redox wave, indicating its high electrocatalytic activity. These results were consistent with that of EIS, which proved this well-defined Au-ZnO film possessed the requisite surface structure and electronic properties to support rapid electron transfer for this sensing system. The nanocomposite could offer effective sensing platform for the sensitive electrochemical determination of DA.

3.3. Effect of pH

To optimize the determination conditions of DA, the effects of pH value on the electrochemical response of DA at the Au-ZnO/GCE was studied by cyclic voltammetry in 0.1 M PBS with the pH range of 5.0-9.0. As shown in Fig. 4A, the CVs of DA at the HAu-G/GCE show a strong dependence on the pH values of solutions. It is observed that the anodic peak current increased with increasing pH value until it reached 7.0; however, the anodic peak current decreased remarkably when the pH was greater than 7.0 (Fig. 4B). Therefore, the PBS of pH 7.0 was selected as the electrolyte in the following experiments.

Fig. 4

In addition, Fig. 4A also shows the relationship between the peak potentials of DA and the pH values. It can be found that peak potential shifted toward negative values

when the pH values increased from 5.0 to 9.0, indicating that protons participate in the electrode reaction. The formal potential (E^{θ}), defined as (E_{pa} + E_{pc})/2, is proportional to the pH (Fig. 4B). The linear regression equation is E^{θ} (V) = 0.42 - 0.04 pH with a correlation coefficient of R^2 = 0.997.

3.4. Effect of scan rate

The effect of scan rate on the anodic peak current (Ipa) of DA was studied by cyclic voltammetry (CV). Fig. 5 shows the CVs of the Au-ZnO/GCE in 0.1 M PBS solutions containing 50 μM DA at different scan rates. With the scan rate increasing, the anodic peak current (I_{pa}) of Au-ZnO/GCE in the DA solution increased. Good linearity

Fig. 5

between the scan rate and the peak current is obtained within the range from 10 to 700 mVs^{-1} (inset of Fig. 5), suggesting an adsorption-controlled reaction process of DA on the modified electrode surface. In addition, the oxidation peak potential (Ep, V) shifts positively with increasing ν, revealing an irreversible oxidation process of DA.

3.5. Electrochemical detection of DA

Fig. 6 shows the DPVs obtained at Au-ZnO/GCE for the concentrations of DA ranging from 0.1 μM to 300 μM in pH 7.0. The corresponding graph of anodic peak

Fig. 6

current versus concentration of DA shows linear relationship. The correlation coefficient for the linearity was 0.9983 for the Au-ZnO/GCE, as shown in inset of Fig. 5. The limit of detection (LOD) is calculated to be 0.02 μM based on the signal-to-noise ratio of 3. (S/N= 3). Compared with the analytical data in literatures,

the fabricated electrochemical sensor was more comparable and exhibited a relatively lower detection limit (listed in Table 1).

Table 1

UA is the most important interference for electrochemical detection of DA. The selective detection and determination of DA in the presence of higher concentrations of UA is difficult at bare unmodified solid electrodes because the oxidation of UA occurred at a potential close to that of DA. The separation of the oxidation peak potentials between DA and UA plays an important role for the analysis of DA in the presence of UA. In the biological fluids, the normal concentration range of UA is about 10^{-4} M. So, the interfering influences of 400 μM UA were studied in PBS (pH 7.0). As shown in Fig. 7, when 130 μM DA and 400 μM UA were coexisted in the same PBS, two separate anodic oxidation peaks were identified with the well peak

Fig. 7

separation. The anodic oxidation potentials were 0.234 V and 0.516 V for DA, and UA, respectively. The peak-to-peak separations between DA and UA were 282 mV, which are large enough to determine DA selectively.

3.6. Repeatability, stability and reproducibility

To evaluate the repeatability of the Au-ZnO/GCE, the peak currents of 20 successive measurements by DPV in a 50 μM DA solution was determined once in 0.5 h. The relative standard deviation (RSD) of 2.1% was obtained. When the modified electrode was used intermittently and stored at ambient temperatures in PBS solution for more than 20 days, the current signals showed less than 3.6% decrease

relative to the initial response. Six parallel-made Au-ZnO/GCEs were used to detect 50 μM DA, respectively. The RSD of the sensor was 2.8%. These results indicate a satisfactory repeatability, reproducibility and stability could be obtained by this novel electrochemical sensing platform.

3.7 Real-world sample analysis

In order to evaluate the practical applicability of the as prepared sensors, it was applied for the detection of DA in urine samples. Urine samples of healthy individuals were frozen until determination and diluted to 1:200. The results are shown in Table 2. The total DA content in urine was 2.00×10^{-6} M. Standard addition methods were

Table 2.

used for testing recoveries and the recoveries in the range of 94.0-104.0% were obtained with the RSDs of 2.6-3.8%.

4. Conclusions

In this work, we successfully fabricated a simple and sensitive electrochemical dopamine sensor by immobilizing nanosheet-based 3D hierarchical ZnO structure decorated with Au nanoparticle on GCE. The as-prepared electrode displayed low detection limit, good reproducibility and high stability. Additionally, such a novel sensor may be employed in the selective and simultaneous determination of dopamine and uric acid in their binary mixture. The successful application of this electrode indicates that Au-ZnO nanocomposite provide a new platform for designing biosensor to determine dopamine sensitively and selectively.

Acknowledgment

The authors are grateful for the financial support provided by National High Technology Research and Development Program of China (No. 2012AA02A404), National Natural Science Foundation of China (No. 51173146), basic research fund of Northwestern polytechnical university (JC20120248) and the Natural Science Foundation of Henan Province (nos. 132300410406).

References:

1. B.J. Venton, R.M. Wightman, Psychoanalytical electrochemistry: Dopamine and behavior , Analytical Chemistry 75(2003), 414A–421A
2. M.K. Zachek, A. Hermans, R.M. Wightman, G.S. McCarty, Electrochemical dopamine detection: Comparing gold and carbon fiber microelectrodes using background subtracted fast scan cyclic voltammetry, Journal of Electroanalytical Chemistry 614 (2008), 113–120.
3. E. Baldrich, R. Gmez, G. Gabriel, F.X Muñoz., Magnetic entrapment for fast, simple and reversible electrode modification with carbon nanotubes: Application to dopamine detection , Biosensors & Bioelectronics, 26 (2011), 1876–1882.
4. J. Szopa, G. Wilczyński, O. Fiehn, A. Wenczel, L. Willmitzer, Identification and quantification of catecholamines in potato plants (Solanum tuberosum) by GC–MS, Phytochemistry 58 (2001) 315–320.
5. R.R. González, R.F. Fernández, J.L.M. Vidal, A.G. Frenich, M.L.G. Pérez, Development and validation of an ultra-high performance liquid chromatography–tandem mass-spectrometry (UHPLC–MS/MS) method for the simultaneous determination of neurotransmitters in rat brain samples, J.Neurosci. Meth. 198 (2011) 187-194.

6. M.R. Moghadam, S. Dadfarnia, A.M.H. Shabani, P. Shahbazikhah, Chemometric-assisted kinetic–spectrophotometric method for simultaneous determination of ascorbic acid, uric acid, and dopamine , Anal. Biochem.410 (2011) 289–295.

7. L. Zhang, N. Teshima, T. Hasebe, M. Kurihara, T. Kawashima, Flow-injectiondetermination of trace amounts of dopamine by chemiluminescence detection, Talanta 50 (1999) 677–683.

8. R. Torabi, R.G. Compton, A simple electroanalytical methodology for the simultaneous determination of dopamine, serotonin and ascorbic acid using an unmodified edge plane pyrolytic graphite electrode, Analytical and Bioanalytical Chemistry 387 (2007) 2793–2800.

9. K. Wu, J. Fei, S. Hu, Simultaneous determination of dopamine and serotonin on a glassy carbon electrode coated with a film of carbon nanotubes, Analytical Biochemistry 318 (2003) 100–106.

10. C.L. Sun, H.H. Lee, J.M. Yang, C.C. Wu, The simultaneous electrochemical detection of ascorbic acid, dopamine, and uric acid using graphene/size-selected Pt nanocomposites, Biosensors and Bioelectronics 26 (2011) 3450–3455.

11. D.P. Quan, D.P. Tuyen, T.D. Lam, P.T.N. Tram, N.H. Binh, P.H. Viet, Electrochemically selective determination of dopamine in the presence of ascorbic and uric acids on the surface of the modified Nafion/single wall carbon nanotube/poly(3-methylthiophene) glassy carbon electrodes, Colloids Surf.,B 88 (2011) 764–770.

12. D. Jia, J. Dai, H. Yuan, L. Lei, D. Xiao, Selective detection of dopamine in the presence of uric acid using a gold nanoparticles-poly(luminol) hybrid film and multi-walled carbon nanotubes with incorporated β-cyclodextrin modified glassy carbon electrode, Talanta 85 (2011) 2344–2351.

13. S. L, J. Yan, G.W. He, D.D. Zhong, J.X. Chen, L.Y. Shi, X.M. Zhou, H.J. Jiang, Layer-by-layer assembled multilayer films of reduced graphene oxide/gold nanoparticles for the electrochemical detection of dopamine, Journal of Electroanalytical Chemistry 672 (2012) 40–44.

14. C.Y. Li, Y. J. Cai, C. H. Yang, C. H. Wu, Y. Wei, T. C. Wen, T. L. Wang, Y. T. Shieh, W. C. Lin, W. J. Chen, Highly sensitive and selective electrochemical determination of dopamine and ascorbic acid at Ag/Ag_2S modified electrode, Electrochim. Acta 56 (2011) 1955–1959.

15. Y. Tong, Z. C. Li, X. F. Lu, L. Yang, W. N. Sun, G. D. Nie, Z. J. Wang, C. Wang, Electrochemical determination of dopamine based on electrospun CeO_2/Au composite nanofibers, Electrochimica Acta 95 (2013) 12– 17.

16. Y. Fan, H.T. Lu, J. H. Liu, C. P. Yang, Q. S. Jing , Y. X. Zhang, X. K. Yang, K. J. Huang, Hydrothermal preparation and electrochemical sensing properties of TiO_2–graphene nanocomposite, Colloids and Surfaces B: Biointerfaces 83 (2011) 78–82

17. Q. Qiao , B. H. Li, C. X. Shan, J. S. Liu, J. Yu, X. H. Xie, Z. Z. Zhang, T. B. Ji, Y. Jia, D. Z. Shen，Light-emitting diodes fabricated from small-size ZnO quantum dots, Materials Letters, 74 (2012), 104-106

18. J. Jean , S. Chang , P. R. Brown , J. J. Cheng , P. H. Rekemeyer, M. G. Bawendi, S. Gradecak , and V. Bulovic, ZnO Nanowire Arrays for Enhanced Photocurrent in PbS Quantum Dot Solar Cells, Advanced Materials, 25 (2013) 2790-2796.

19. Y. T. Shi, C. Zhu, L. Wang, Ch. Y. Zhao, W. Li, K. K. Fung, T. L. Ma, A. Hagfeldt, and N. Wang, Ultrarapid Sonochemical Synthesis of ZnO Hierarchical Structures: From Fundamental Research to High Efficiencies up to 6.42% for Quasi-Solid Dye-Sensitized

Solar Cells, Chem. Mater, 25(2013) 1000-1012.

20. H. Zhu, C. X. Shan, J.Y. Zhang, Z. Z. Zhang, B. H. Li, D. X. Zhao1, B. Yao, D. Z. Shen, X.W. Fan, Z. K. Tang, X. H. Hou, K. L. Choy, Low-Threshold Electrically Pumped Random Lasers, Advanced Materials, 16 (2010) 1877-1883

21. H. Zhu, C. X. Shan, B. Yao, B. H. Li, J. Y. Zhang, Z. Z. Zhang, D. X. Zhao, D. Z. Shen, X. W. Fan, Y. M. Lu, Z. K. Tang, Ultralow-Threshold Laser Realized in Zinc Oxide, Advanced Materials, 16 (2009) 1613-1618

22. X. b. Zhao, G. M. Ashley, L. G. Gancedo, H. Jin, J. K. Luo, A. J. Flewittd, J. R. Lu, Protein functionalized ZnO thin film bulk acoustic resonator as an odorant biosensor, Sensors and Actuators B, 163 (2012) 242-247.

23. L. L. Xie, Y. D. Xu, X.Y. Cao, Hydrogen peroxide biosensor based on hemoglobin immobilized at graphene, flower-like zinc oxide, and gold nanoparticles nanocomposite modified glassy carbon electrode, Colloids and Surfaces B: Biointerfaces, 107 (2013) 245–250.

24. M.G. Zhao, Z.L. Li, Z. Q. Han, K. Wang, Y. Zhou, J. Y. Huang, Z. Z. Ye, Synthesis of mesoporous multiwall ZnO nanotubes by replicating silk and application for enzymatic biosensor, Biosensors and Bioelectronics, 49 (2013) 318–322.

25. P. Nayak , B. Anbarasan , and S. Ramaprabhu , Fabrication of organophosphorus biosensor using ZnO nanoparticle-decorated carbon nanotube-graphene hybrid composite prepared by a novel green technique, J. Phys. Chem. C, 117 (2013), 13202–13209

26. K. Jindal, M. Tomar and V. Gupta, Nitrogen-doped zinc oxide thin films biosensor for determination of uric acid, Analyst, 138 (2013) 4353-4362

27. J.Y. Kim, S.Y. Jo, G. J. Sun, A. Katoch, S. W. Choi, S. S. Kim, Tailoring the surface area of ZnO nanorods for improved performance in glucose sensors, Sensors and Actuators B: Chemical, 192 (2014) 216–220

28. S. Chawla, C. S. Pundir, An amperometric hemoglobin A1c biosensor based on immobilization of fructosyl amino acid oxidase onto zinc oxide nanoparticles-polypyrrole film , Anal. Biochem, 430 (2012) 156-162.

29. D. J. Gargas, H. W. Gao, H. T. Wang, and P. D. Yang, High quantum efficiency of band-edge emission from ZnO nanowires, Nano Lett, 11 (2011) 3792-3796.

30. H.G. Yang, C.H. Sun, S.Z. Qiao, J. Zou, G. Liu, S.C. Smith, H.M. Cheng, G.Q. Lu, Anatase TiO_2 single crystals with a large percentage of reactive facets, Nature 453 (2008) 638-641.

31. J. Zhang, J.G. Yu, Y. Zhang, Q. Li, J.R. Gong, Visible light photocatalytic H_2-production activity of CuS/ZnS porous nanosheets based on photoinduced interfacial charge transfer , Nano Letters 11 (2011) 4774-4779.

32. R. Chai, R. Yuan, Y.Q. Chai, C.F. Ou, Amperometric immunosensors based on layer-by-layer assembly of gold nanoparticles and methylene blue on thiourea modified glassy carbon electrode for determination of human chorionic gonadotrophin, Talanta 74 (2008) 1330–1336.

33. A.I. Gopalan, K.P. Lee, K.M. Manesha, P. Santhosha, Gold nanoparticles dispersed into poly(aminothiophenol) as a novel electrocatalyst-fabrication of modified electrode and evaluation of electrocatalytic activities for dioxygen reduction, Journal of Molecular Catalysis A 256 (2006) 335–345.

34. S. L. Yang, Y. L. Yin, G. Li, R. Yang, J. J. Li , L. B. Qua, Immobilization of gold nanoparticles on multi-wall carbon nanotubes as an enhanced material for selective voltammetric determination of dopamine, Sensors and Actuators B 178 (2013) 217– 221.

35. W. C. Zhu, T. Chen, X. M. Ma, H. Y. Ma, S. H. Chen, Highly sensitive and selective detection of dopamine based on hollow gold nanoparticles-graphene nanocomposite modified electrode, Colloids and Surfaces B: Biointerfaces 111 (2013) 321– 326

36. C. Y. Wang, F. C. Ye, H. F. Wu, Y. Qian, Depositing Au nanoparticles onto graphene sheets for simultaneous electrochemical detection ascorbic acid, dopamine and uric acid, Int. J. Electrochem. Sci., 8 (2013) 2440 – 2448.

37. C. L. Zhou, S. Li, W. Zhu, H. J. Pang, H. Y. Ma, A sensor of a polyoxometalate and Au–Pd alloy for simultaneously detection of dopamine and ascorbic acid, Electrochimica Acta 113 (2013) 454-463.

38. F. Xiao, F.Q. Zhao, J.W. Li, L.Q. Liu, Characterization of hydrophobic ionic liquid carbon nanotubes–gold nanoparticles composite film coated electrode and the simultaneous voltammetric determination of guanine and adenine, Electrochimica Acta 53 (2008) 7781–7788.

39. A.I. Gopalan, K.P. Lee, K.M. Manesha, P. Santhosh, Electrochemical determination of dopamine and ascorbic acid at a novel gold nanoparticles distributed poly(4-aminothiophenol) modified electrode, Talanta 71 (2007) 1774D–1781D.

40. X.Q. Tian, C.M. Cheng, H.Y. Yuan, J. Dua, Simultaneous determination of L-ascorbic acid, dopamine and uric acid with gold nanoparticles-cyclodextrin-graphene-modified electrode by square wave voltammetry, Talanta 93 (2012) 79–85.

41. G.Z. Hu, D.P. Zhang, W.L. Wu, Z.S. Yang, Selective determination of dopamine in the presence of high concentration of ascorbic acid using nano-Au selfassembly glassy carbon electrode, Colloid Surface B 62 (2008) 199–205.

42. L. X. Fang, B. L. Zhang, W. Li, X. J. Li, T. J. Xin, Q. Y. Zhang, Time-dependent control of phase and morphology transformation of porous ZnO hollow microsphere by a facile one-step solution route RSC Adv., 2014, 4, 7167-7173.

43. X. Cao, N. Wang, L. Wang, L. Guo, Synthesis of nanochain-assembled ZnO flowers and their application to dopamine sensing, Sensors and Actuators B 147 (2010) 629–634.

44. Chun-Fang Tang, S. Ashok Kumar, Shen-Ming Chen, Zinc oxide/redox mediator composite films-based sensor for electrochemical detection of important biomolecules, Analytical Biochemistry 380 (2008) 174–183.

45. G.P. Jin, X.Q. Lin, J.M. Gong, Novel choline and acetylcholine modified glassy carbon electrodes for simultaneous determination of dopamine, serotonin and ascorbic acid, Journal of Electroanalytical Chemistry 569 (2004) 135–142.

461 Table 1 Comparison between the proposed sensor and other reported sensor for DA detection.

Electrode materials	Linear range (μM)	LOD (μM)	References
β-CD-MWCNTs/Plu-AuNPs	1.00-50	0.380	12
{AuNPs/RGO}20	1.00-60.0	0.0200	13
Ag_2S	1.00-10.0	1.00	14
CeO_2/Au composites nanofibers	10.0-500	0.0560	15
TiO_2-graphene nanocomposites	5.00-200	2.00	16
Nanochain-assembled ZnO flowers	0.110-180	0.0600	43
Zinc oxide/redox mediator composites	6.00-120	0.500	44
5-Hydroxytryptophan	0.500-30.0	0.310	45
Au-ZnO nanocomposites	0.100-300	0.0200	In this work

462

463 Table 2 Determination of DA in human urine sample with developed method (*n*=5).

Sample	No spiked (μM)	Added (μM)	Found[a] (μM)	Recovery (%)	RSD (%)
1	0.0100	0.500	0.500	98.0	3.30
2	-	0.500	0.480	96.0	3.80
3	0.0100	0.500	0.520	104	2.60
4	-	0.500	0.470	94.0	3.00
5	-	0.500	0.480	96.0	2.80
6	0.0200	0.500	0.510	102	3.60
7	-	0.500	0.490	98.0	3.10

464 [a] RSD for 5 repetitive measurements

Figure captions

Fig.1. (a) low magnification FESEM image of ZnO microsphere, (b) high-magnification FESEM image of ZnO microsphere, (c) high-magnification FESEM images of Au-ZnO nanocomposite, (d) EDS spectra of Au-ZnO nanocomposite, (e) HRTEM image of Au-ZnO nanocomposite, the inset is TEM image of Au-ZnO nanocomposite. (f) XRD pattern (curve a) of the ZnO microspheres and XRD pattern (curve b) of Au-ZnO nanocomposite

Fig. 2 The electrochemical impedance spectroscopy (EIS) of bare GCE (a), Au-ZnO (b), ZnO (c), in 0.1 M KCl aqueous solution containing 5.0 mM $[Fe(CN)_6]^{3-/4-}$. The frequency range is from 0.1 Hz to 100 KHz at the formal potential of 0.2 V. The inset A represents the Randles equivalent circuit model for the impedance of the electrochemical sensing system. The inset B is the enlarged view of curve a.

Fig. 3 In PBS solution (0.1 M, PH 7.0), CVs of Au-ZnO/GCE without DA (a) and ZnO/GCE (b), GCE (c), Au-ZnO/GCE (d) for 50 μM DA. Scan rate:100 mV s^{-1}.

Fig. 4 At the Au-ZnO/GCE electrode, cyclic voltammograms of 50 μM DA in different pH solutions (a) 5; (b) 6; (c)7; (d) 8 and (e) 9 (from right to left) (A), and the dependences of the DA oxidation peak current and redox potential on the PBS solution pH with a scanning rate of 100 mVs^{-1} (B).

Fig. 5 Cyclic voltammograms of 50 μM DA at Au-ZnO/GCE in PBS (PH 7.0) at various scan rates: inner to outer are 10-700 mVs^{-1}. Inset to (B) shows the linear dependence of peak currents with scan rate.

Fig. 6. DPV profiles at Au-ZnO/GCE in 0.1M PBS (PH 7.0) different concentrations

of DA: 0.1, 5, 20, 40, 80, 130, 180, 240 and 300 μM (from a to i). Scan rate: 100 mV s^{-1}. Inset: the calibration curve for the determination of DA;

Fig. 7 The effect of UA on the DPV response of DA: 130 μM DA (a), 130 μM DA and 400 μM UA (b) at Au-ZnO/GCE in 0.1 M PBS (pH 7.0)

Fig. 1

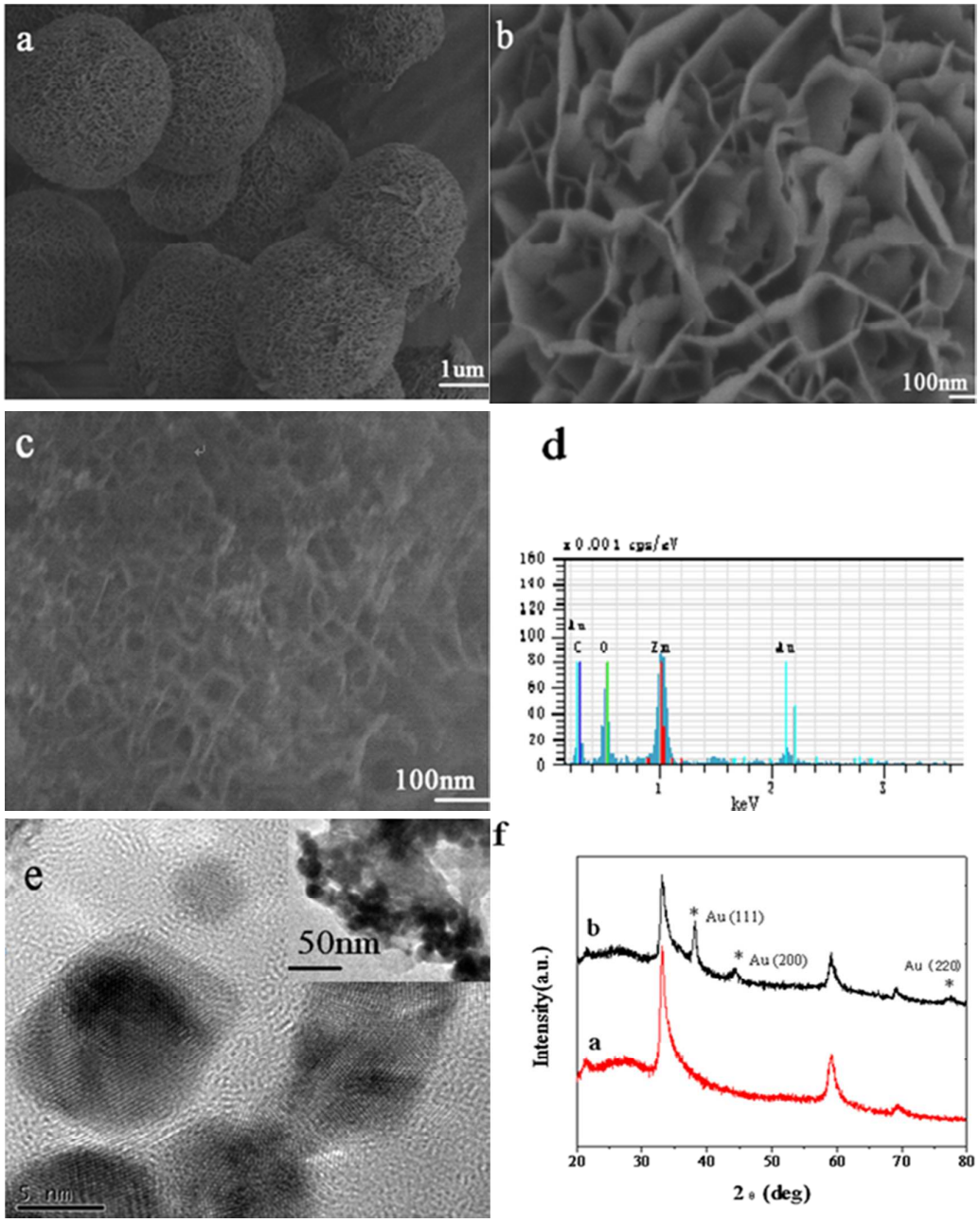

518 Fig. 2

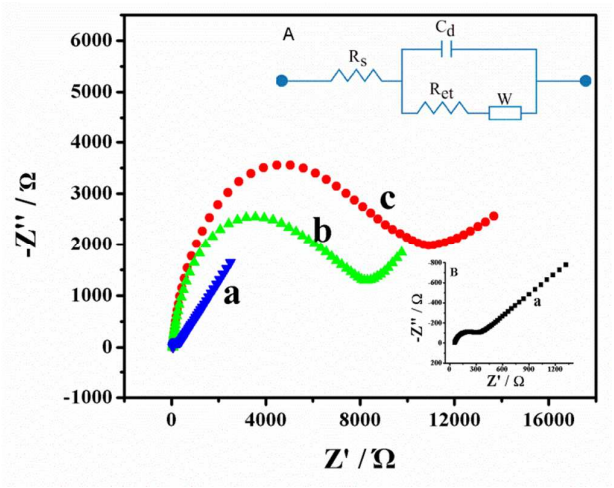

519

520 **Fig.3**

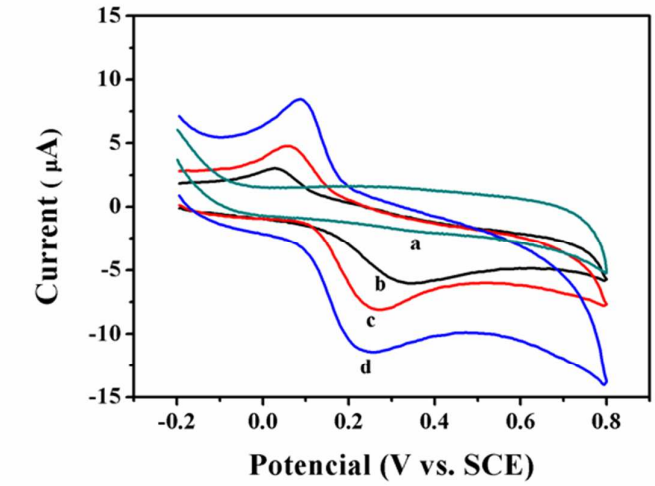

521

522

523

524

525

526 **Fig.4**

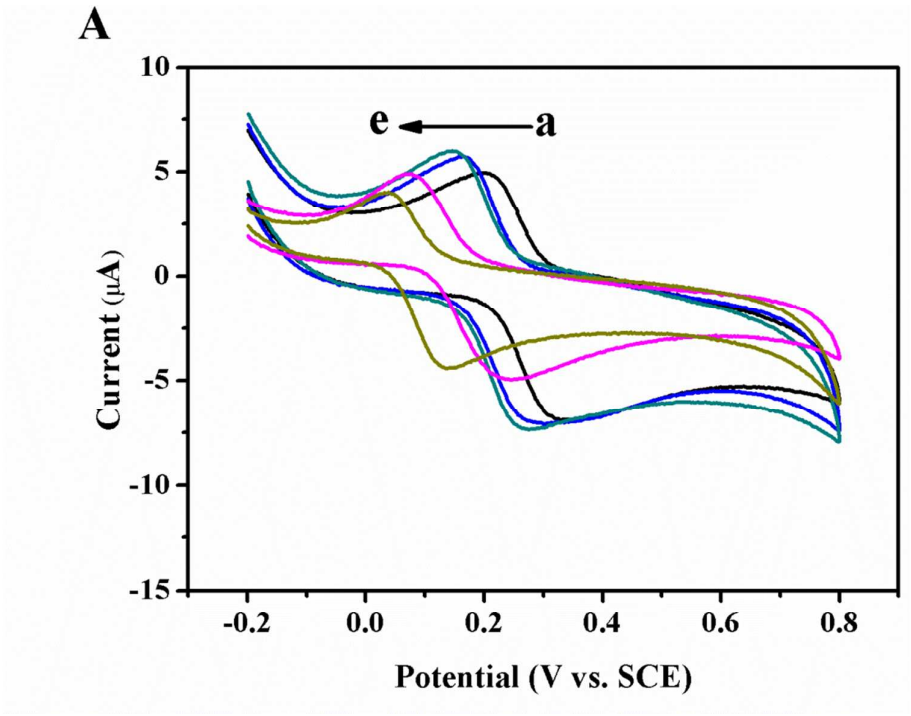

527

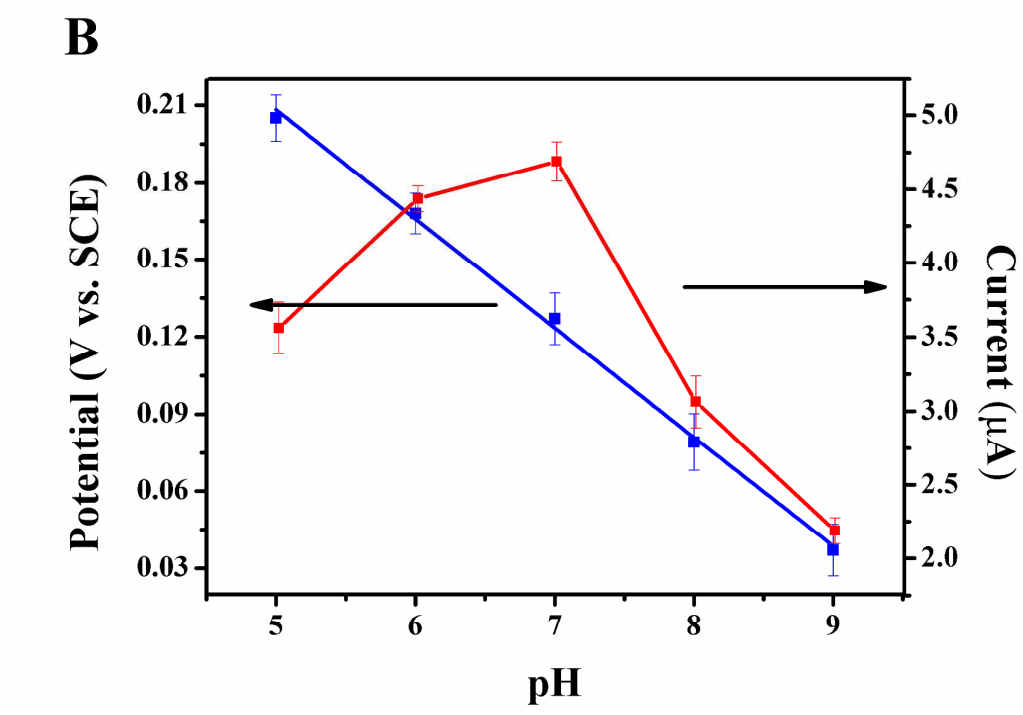

528

529

530

531 **Fig.5**

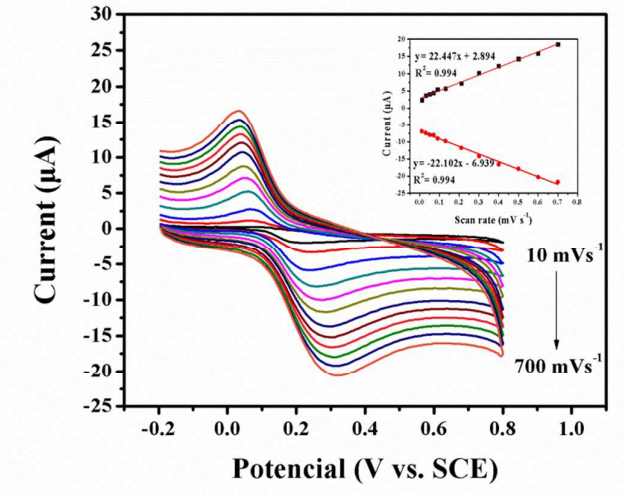

532

533 Fig.6

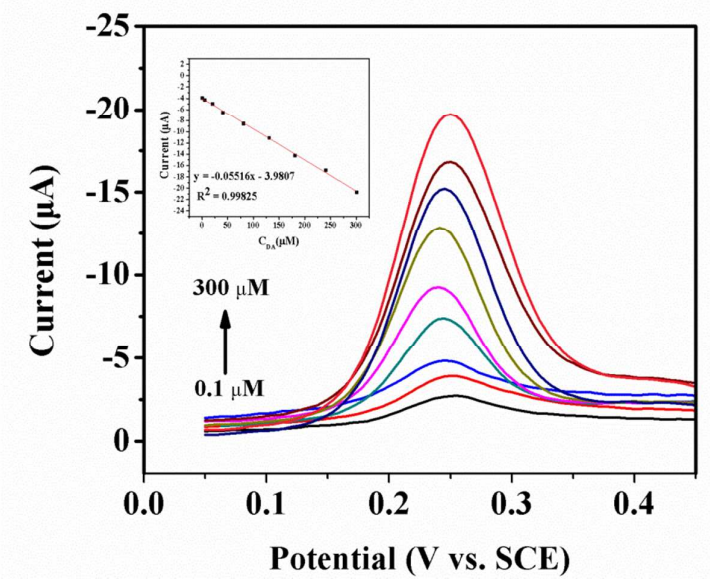

534

535

536

537

538 Fig.7

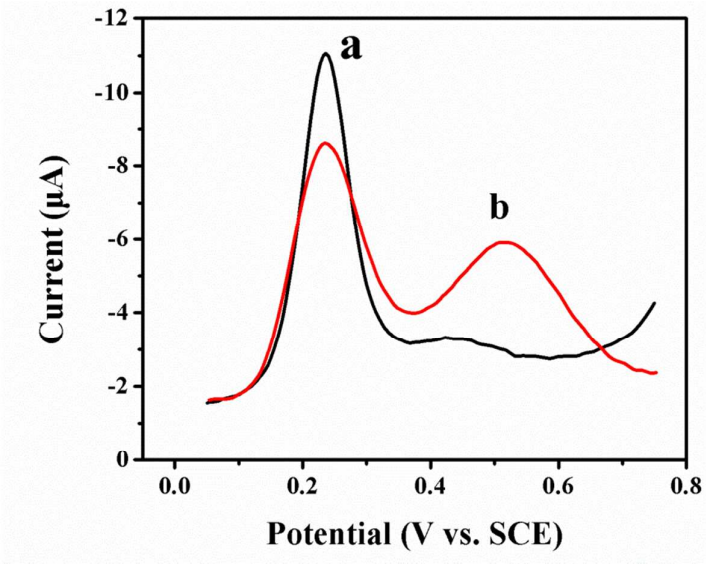

539

540